# Flash Graphene from Plastic Waste

Wala A. Algozeeb,[1] Paul E. Savas,[1] Duy Xuan Luong,[1] Weiyin Chen,[1] Carter Kittrell,[1] Mahesh Bhat,[2] Rouzbeh Shahsavari,[2] and James M. Tour[*,1,3,4]

[1]Department of Chemistry, Rice University, 6100 Main Street, Houston, Texas 77005, USA

[2]C-Crete Technologies, Stafford, TX, USA

[3]Department of Materials Science and NanoEngineering, Rice University, 6100 Main Street, Houston, Texas 77005, USA

[4]Smalley-Curl Institute, NanoCarbon Center and Welch Institute for Advanced Materials, Rice University, 6100 Main Street, Houston, Texas 77005, USA

*Email: tour@rice.edu

**Abstract** In this work, an approach to upcycling plastic waste (PW) products is presented. The method relies on flash Joule heating (FJH) to convert PW into flash graphene (FG). In addition to FG, the process results in the formation of carbon oligomers, hydrogen, and light hydrocarbons. In order to make high quality graphene, a sequential alternating current (AC) and direct current (DC) flash is used. The FJH process requires no catalyst and works for PW mixtures, which makes the process suitable for handling landfill PW. The energy required to convert PW to FG is ~ 23 kJ/g or ~ \$125 in electricity per ton of PW, potentially making this process economically attractive for scale-up. The FG was characterized by Raman spectroscopy and had a $I_{2D}/I_G$ peak ratio up to 6 with a low-intensity D band. Moreover, transmission electron microscopy and X-ray diffraction analysis show that the FG is turbostratic with an interlayer spacing of 3.45 Å. The large interlayer spacing will facilitate its dispersion in liquids and composites. Analysis of FG dispersions in 1% Pluronic aqueous solution shows that concentrations up to 1.2 mg/mL can be achieved. The carbon

oligomers that distilled from the process were characterized by Fourier-transform infrared spectroscopy and have chemical structures similar to the starting PW. Initial analysis of gas phase products shows the formation of considerable amounts of hydrogen along with other light hydrocarbons. Since graphene is naturally occurring and it shows a low toxicity profile, this could be an environmentally beneficial method to upcycle PE.

**Keywords** plastic waste, microplastics, recycling, upcycling, graphene, composites.

Plastic waste (PW) pollution is becoming one of the most pressing environmental concerns in the 21st century.[1] A large fraction of PW ends up in landfills and the ocean, leading to the formation of micro- and nano-plastics that threaten marine life,[2] microorganisms,[3, 4] useful bacteria,[3] and humans.[5, 6] In addition, plastics production from petrochemicals has a high carbon footprint.[7] Crude oil must be extracted, distilled, refined, and purified to form petrochemical feedstocks that are further processed to produce plastic in complex and energy-intensive facilities that emit a large amount of greenhouse gases.[8] Additional greenhouse gases are emitted during the shaping of plastic for use and when transporting to customers. After this intense carbon footprint process, most of the synthesized plastic is used only once before dumping into over-stressed landfills or waterways that terminate in oceans.[7] Thus, upcycling PW to higher value materials and chemicals is environmentally and economically advantageous.

To reduce the amount of PW, much effort has been directed toward physical recycling, in which the plastic is detergent-washed multiple times and reshaped for reuse. However, physical recycling has major drawbacks including the need for human-labor intensive sorting of plastics prior to

milling, grinding, and sterilizing.[9-11] Another route for PW handling is chemical recycling, where PW is pyrolyzed in an inert atmosphere, sometimes in the presence of a catalyst, decomposing the plastic into smaller molecules and oils.[12-15] Moreover, PW pyrolysis involves heating large reactors up to 500-600 °C,[15] consuming sizable amounts of energy while making chemical formation expensive with a large carbon footprint.[16] Another drawback of chemical recycling is the poisoning of the catalyst during the pyrolysis process due to the presence of contaminants in PW, such as additives and plasticizer. For this reason, PW must be pretreated to extract inorganic additives prior to chemical recycling to avoid catalyst poising. To date, most reported recycling technologies are not cost-effective and thus only 9% of all produced plastic has been recycled.[17,18] Therefore, greener recycling or upcycling technologies are sought; the latter occurring when the products attain a higher value than the starting plastic.

This work describes an alternative approach to chemical and physical recycling when dealing with PW and it is based upon our recently developed direct current (DC) flash Joule heating (DC-FJH) method (Figure S1) to convert carbon sources into graphene; the process forming what is called flash graphene.[19] The technology relies on electricity to induce FJH in PW. This drives the carbon source to high temperatures in a short time period. The work here shows that alternating current (AC) flash Joule heating (AC-FJH) (Figure S2) is advantageous over DC-FJH when dealing with PW because it can be sustained for seconds, 8 s in this case. This permits the release of the necessary volatiles, producing an intermediate AC flash graphene (AC-FG) with a $I_{2D}/I_G$ peak ratio between 1.2 and 0.5 and a high-intensity D band when characterized by Raman spectroscopy. This process overcomes the need to pyrolyze the plastic in furnaces where much of the energy is lost in the process. Then, upon a single DC-FJH pulse, the intermediate AC-FG is converted to very high-

quality turbostratic FG (tFG) with $I_{2D}/I_G$ peak ratio between 1 and 6 and low-intensity D band when characterized by Raman spectroscopy. This sequential AC and DC (ACDC) flash process was shown to be effective for upcycling both single-stream thermoplastics and PW mixtures. Given the high stability of graphene to typical microbial,[20,21] chemical,[22] and thermal degradation,[23] this technology offers a method for converting PW into a stable and naturally occurring form of carbon that has low toxicity.[24, 25] Agglomerates of graphene are the natural mineral graphite.

**Results and Discussion**

PW was ground using a commercial grinder and mixed with 5 wt% carbon black (CB) to obtain a conductive mixture. The CB can be substituted with 5 wt% FG from a former run. The plastic powder was packed in a quartz tube between two copper electrodes and was treated with AC-FJH (120 V, 60 Hz) for 8 s. An outline of the AC-FJH circuit is shown in Figure 1a. Pictures and electrical schematic of the AC-FJH equipment are in Figure S2. During the AC-FJH, the conductive PW sample releases carbon oligomers and volatiles while FG is formed between the copper electrodes. The electrodes can also be made from graphite or other conductive refractory materials. There is ~0.5 mm of space between the electrodes and the quartz sidewall allowing for the volatiles to escape from the quartz tube. All flashing procedures must take place inside an evacuated closed chamber for safety (see safety notes in the Supporting Information). FG obtained from the AC-FJH process is termed AC-FG. Plastic powders with different particle sizes were used to find that a powder with grain size between 1 mm and 2 mm gives the highest yield of AC-FG when 5% CB is used. Plastic powders with grain size larger than 2 mm are not conductive enough to react when mixed with 5 wt% CB, while powders with grain size smaller than 50 µm

tend to escape from the quartz tube, with its loose fitting electrodes, during the FJH process, causing a large drop in the yield of AC-FG. Figure 1b shows the yield of AC-FG when 2 mm, 1 mm and 40 μm particles of high-density polyethylene (HDPE) powders were separately subjected to AC-FJH to obtain 23%, 21% and 10% AC-FG yield, respectively. Another factor that plays an important role in the yield of AC-FG is the initial resistivity across the sample; compressing the plastic powders into the quartz tube lowers the initial resistivity and increases the FG yield. Figure 1c shows the yield of AC-FG obtained from flashing HDPE powder at different initial resistivity derived from different sample compressions between the two electrodes. AC-FJH was found to be useful for FG production from different thermoplastics including: polyethylene terephthalate (PET), HDPE, poly(vinyl chloride) (PVC), low density polyethylene (LDPE), polypropylene (PP), and polystyrene (PS); the FG yield varied based on the parent material. As shown in Figure 1d, the yield of AC-FG obtained from different thermoplastics was found to correlate to the thermal stability of the parent material; the higher the thermal stability of the plastic, the higher the FG yield and the less volatile oligomers generated. Note that the yields were calculated based on the carbon content of the polymer. Added CB converts to FG upon FJH, contributing <4% to the total yield. Figure 1e shows large shreds of post-consumer HDPE plastic from a commercial recycler (Polywize, Jacksonville Texas), which was then cut using a commercial cutter, mixed with 5 wt% CB, and finally, after FJH, converted into AC-FG. Unlike plastic pyrolysis processes, there is no need for a high-temperature furnace or catalyst. The AC-FJH process produces an intermediate FG, which is transformed into high quality FG by a short DC-FJH pulse (see below). We tried to flash silica ($SiO_2$) with 5% CB, but the mixture was not conductive enough to flash. After adding 25% CB, the material was conductive enough to flash but did not yield graphene. Thus, silica mixed with up to 25% CB does not produce graphene.
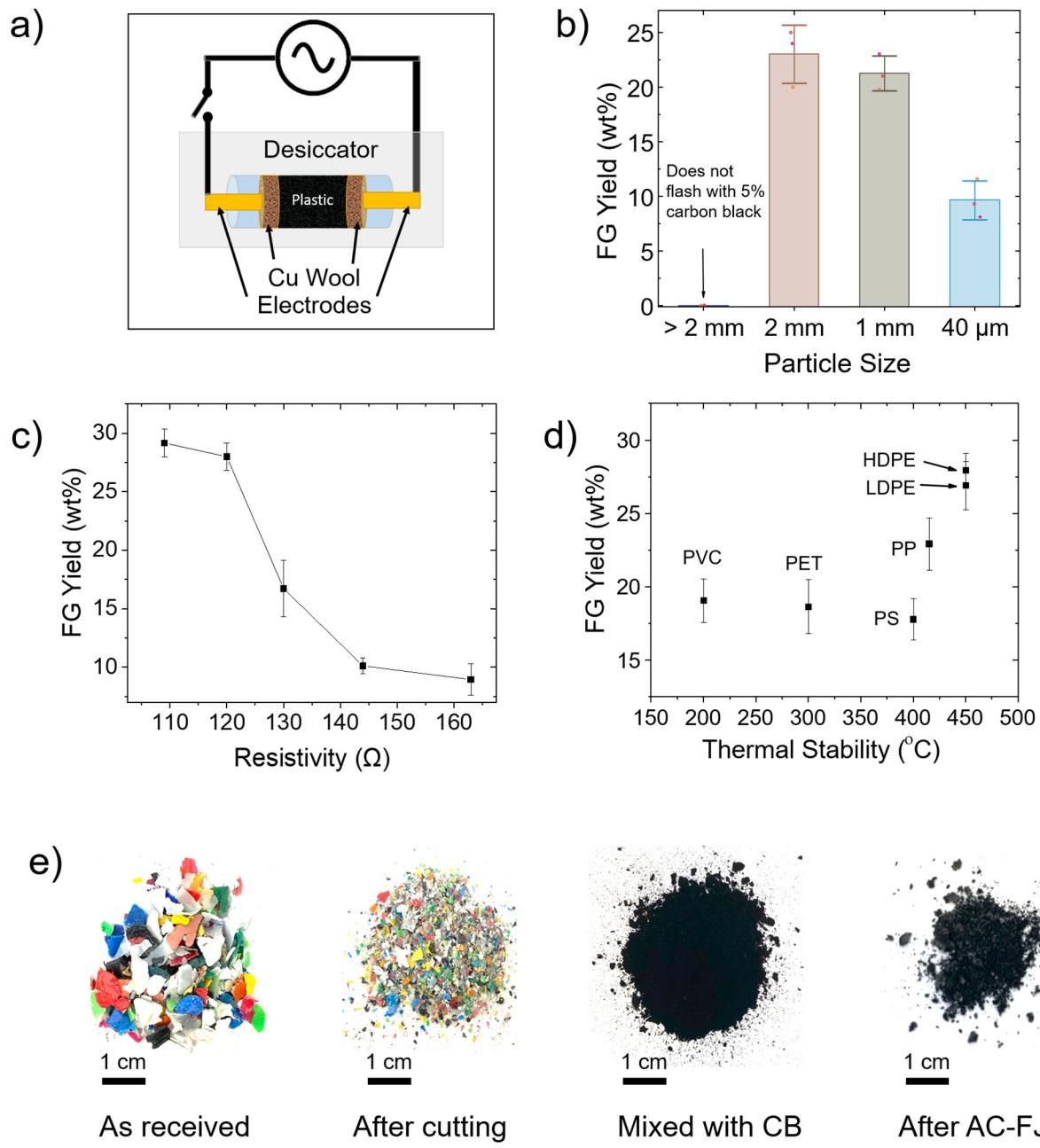
**Figure 1**. a) Schematic of the 120 V AC circuit. b) AC-FG yield from HDPE with 2 mm, 1 mm and 40 μm particle size with 5 wt% CB at initial resistivity of 125 Ω. Samples of particle size >2 mm did not flash with 5% CB. The error bars are standard deviation over 3 sample runs. c) Effect of initial resistivity of HDPE/CB mixture on AC-FG yield. The resistivity is lowered through the

application of increased compression (screw vice) between the two electrodes. The error bars on the graph are standard deviation over 3 sample runs. d) Typical AC-FG yields from different plastics when the initial resistance is 120 $\Omega$. The error bars are standard deviation over 3 sample runs. e) Pictures of (L-R): post-consumer plastic as received from a recycler; after cutting using a commercial cutter; after mixing with 5 wt% CB; and further conversion to FG using AC-FJH.

The quality of FG was determined using Raman spectroscopy. AC-FJH was found to result in the formation of FG with different $I_{2D}/I_G$ peak ratios, as well as different D band intensities. Figure 2a displays the mean characteristic Raman spectrum of FG obtained from the AC-FJH pretreatment process, showing broad 2D and G bands and substantial D bands. The quality of AC-FG was significantly upgraded using a single 500 milliseconds (ms) DC pulse (see Figure S1 for DC circuit outline) to obtain high quality turbostratic FG (tFG) from many kinds of plastic (Figure 2b). tFG obtained from AC-FJH followed by DC-FJH is termed ACDC-tFG. Detailed analysis (Lorentzian fitting) was performed on each of the collected Raman spectra; fitting data may be found in the Figures S3-S14. The collected Raman spectra for both AC-FG and ACDC-tFG have excellent Lorentzian fitting with $R^2 \geq 0.98$, indicating the absence of Bernal stacking.[26] When characterizing tFG, the $I_{G/D}$ peak ratio is an important indicator of the degree of disorder and the quality of tFG. A higher $I_{G/D}$ peak ratio is indicative of a lower degree of disorder and higher tFG quality.[27-29] Figure 2a,b show that the $I_{G/D}$ peak ratio increases significantly in ACDC-tFG when compared to AC-FG. This suggests that the DC-FJH of AC-FG reduces disorder and results in the formation of high-quality tFG. The formation of the low D band could also be indicative of the formation of large sheets with low edge densities and low disorder, or from the formation of zigzag edges that reduce the intensity of the D-band.[30] Table 1 lists the position and the full width half maxima

(FWHM) of the 2D, G, and D band of AC-FG and ACDC-tFG. DC-FJH transforms the quality of AC-FG to obtain sharp 2D and G bands and low D band intensity when characterized by Raman spectroscopy. Upon DC-FJH, the 2D band shifts from 2689 cm$^{-1}$ to 2700 cm$^{-1}$ and the FWHM decreases from 71 cm$^{-1}$ to 27 cm$^{-1}$, resulting in a sharp 2D band that matches the data reported for high-quality turbostratic graphene.[19,31-33] The G band shifts from 1580 cm$^{-1}$ to 1584 cm$^{-1}$ and the FWHM decreases from 44 cm$^{-1}$ to 16 cm$^{-1}$, giving a sharp G band. Unlike typically furnace grown graphene, the $I_{2D}/I_G$ peak ratio is not a good indicator of the quality of tFG. The $I_{2D}/I_G$ peak height ratio is mainly an indicator of the number of turbostratic layers[34] (see Supporting Information for more information about assessing the quality of tFG)

High quality FG is difficult to obtain by direct DC-FJH treatment of PW without the AC-FJH. AC-FJH is essential for removing more volatiles from the PW to obtain high quality FG (see Figure S15 and Figure S16 for Raman spectra and TGA of FG obtained when only DC-FJH was used to make FG from plastics). Figure 2c shows the Raman spectrum of ACDC-tFG from PVC with $I_{2D}/I_G$ peak ratio equal to 6, in which the TS$_1$ and TS$_2$ bands are observed that are indicative of the pure turbostratic morphology of tFG.[32] Previous studies show that turbostratic graphene with some Bernal stacked layers would have a large M-peak that is not observed in our FG.[33] During the AC-FJH processes, the temperature rises to ~2900 K, forcing the C-C bonds to break and rearrange to the more stable graphene. Most excess energy is released *via* light radiation, which results in rapid cooling of the carbon material and a bright flash with every discharge. The fast cooling rate leads to the random arrangement of the graphene sheets to obtain tFG. There is insufficient time to form AB-stacked layers. When the cooling rate was slowed by trapping the IR and UV emissions inside the flashing tube, graphene with a broad 2D peak (FWHM of 65 cm$^{-1}$) and was observed. The

peaks did not show good Lorentzian fitting, indicating the formation of AB-stacked graphene upon slowing the cooling rate (Figure S17). The same phenomena is observed with long DC-FJH pulse durations; longer heating times induce the formation of AB-stacked graphene.[35] Figure 2d shows the temperature profile of the AC-FJH processes collected *via* an in-house built infra-red (IR) spectrometer (spectrometer components are shown in Figure S18). The collected data were fitted with black body radiation curves to find that the temperature rises to 2900 K during AC-FJH process. The DC-FJH flash is known to reach ~3100 K, which is the temperature required to obtain high quality graphene as shown in previous work.[19] Recordings of the current passing through the sample during the DC-FJH process shows that 180 amps of electricity passes through the sample in ~ 100 ms discharge time (Figure S19). FJH to such high temperatures volatilizes non-carbon elements, leaving a highly pure form of graphene. Note that most elements, including metals and silicon,[36] sublime below 2900 K while carbon sublimes ~ 3900 K.[37] This purification mechanism obviates the need to remove contaminates, such as plasticizers, residual food and even clays, before using FJH to obtain high quality FG. For example, PET carbonated beverage bottles contain ~10% nano-clay that is added as a gas barrier.[38] These were subjected to AC-FJH and it was observed that the nano-clays sublime (possibly after reduction) from the PW matrix during the FJH process to produce FG (see Figure S20 for TGA of PET before and after FJH). FJH was shown to be effective for converting PW mixtures to FG, which makes this process a good choice for eliminating the labor-intensive sorting steps necessitated by other recycling/reuse processes.
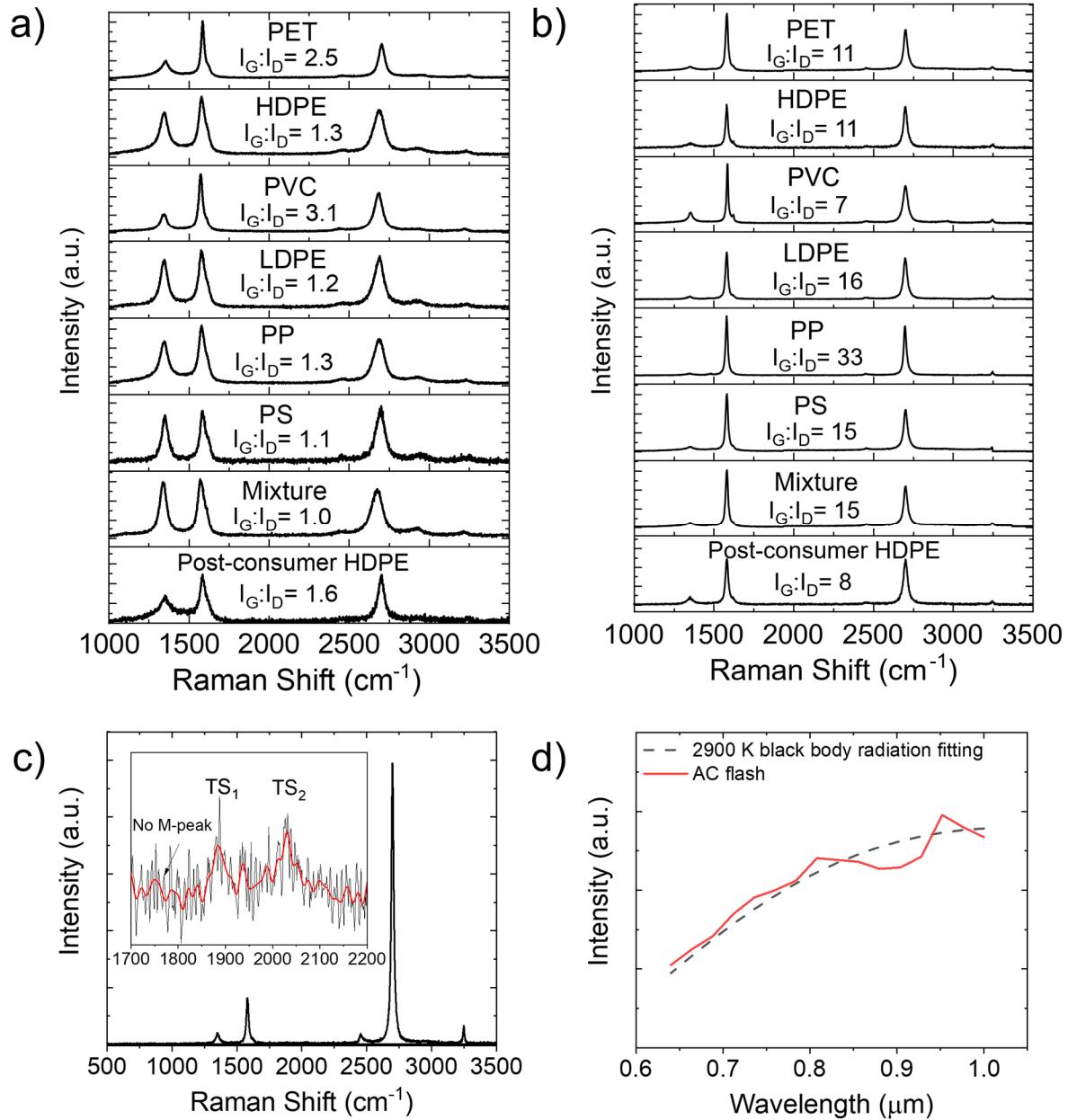
**Figure 2**. Characteristic Raman spectra of a) AC-FG and b) ACDC-tFG. Plastic mixture is 40% HDPE, 20% PP, 20% PET, 10% LDPE, 8% PS, and 2% PVC. c) Raman spectrum of highly turbostratic FG observed for ACDC-tFG from PVC, showing the turbostratic FG bands in the expanded spectrum. d) Temperature profile of the AC-FJH processes collected using an IR spectrometer and blackbody radiation fitting.

**Table 1**. Analysis of the 2D, G and D bands from the Raman spectra.

| | 2D | | | | G | | | | D | | | |
| | AC-FG | | ACDC-tFG | | AC-FG | | ACDC-tFG | | AC-FG | | ACDC-tFG | |
| Plastic Type | Position $(cm^{-1})$ | FWHM $(cm^{-1})$ | Position $(cm^{-1})$ | FWHM $(cm^{-1})$ | Position $(cm^{-1})$ | FWHM $(cm^{-1})$ | Position $(cm^{-1})$ | FWHM $(cm^{-1})$ | Position $(cm^{-1})$ | FWHM $(cm^{-1})$ | Position $(cm^{-1})$ | FWHM $(cm^{-1})$ |
|---|---|---|---|---|---|---|---|---|---|---|---|---|
| PET | 2682 | 63 | 2701 | 31 | 1573 | 32 | 1581 | 18 | 1342 | 55 | 1352 | 62 |
| HDPE | 2686 | 82 | 2701 | 28 | 1581 | 53 | 1581 | 18 | 1343 | 75 | 1350 | 35 |
| PVC | 2682 | 64 | 2700 | 36 | 1573 | 32 | 1586 | 13 | 1342 | 55 | 1354 | 43 |
| LDPE | 2686 | 76 | 2701 | 28 | 1581 | 52 | 1581 | 18 | 1343 | 58 | 1350 | 35 |
| PP | 2686 | 81 | 2699 | 20 | 1581 | 53 | 1581 | 16 | 1343 | 74 | 1350 | 60 |
| PS | 2694 | 70 | 2701 | 18 | 1581 | 46 | 1582 | 18 | 1349 | 45 | 1352 | 62 |
| Average | 2689 | 71 | 2701 | 27 | 1580 | 44 | 1582 | 17 | 1345 | 67 | 1351 | 50 |
| STDV | 7 | 13 | 1 | 7 | 4 | 11 | 2 | 2 | 4 | 17 | 2 | 13 |

X-ray diffraction (XRD) of ACDC-tFG obtained from different PW products shows two peaks occurring at 26.1° (002) and 45° (001) (Figure S21 has XRD of tFG from different plastics). Compared to graphite and graphite nanoplatelets (Figure 3a), both of which have AB stacked layers, ACDC-tFG has a (002) peak that occurs at a slightly lower $2\Theta$ with $I_c = 3.45$ Å, indicating larger interlayer distance between the ACDC-tFG sheets.[19,39,40] The (002) peak of ACDC-tFG has a tail that extends to low $2\Theta$, which is due to rotational disorder between the ACDC-tFG layers.[41] Figure 3b shows the TGA of ACDC-tFG from the HDPE with thermal decomposition commencing at ~625 °C in air. The high thermal stability is indicative of the high degree of crystallinity and low defects of the tFG structure, since defects often lower the thermal stability of graphene.[23] A survey XPS of ACDC-tFG from HDPE shows pure carbon composition without the detectable

presence of heteroatoms (Figure 3c). High-resolution carbon XPS of ACDC-tFG from HDPE (Figure 3d) shows large C-C/C=C peaks occurring at 284.5 eV. Trace C-O/C-O-C and O-C=O XPS peaks were observed at 286.5 eV and 288 eV, respectively. Note that PVC, which has ~ 50% chlorine content, formed high purity FG upon flashing, without a detectable presence of chlorine by high-resolution XPS (Figure S22). This indicates that the FJH method is effective for handling PW that is otherwise difficult to repurpose. When flashing PVC, hydrochloric acid (HCl) is expected to be released during the AC-FJH process as one of byproducts along with other hydrocarbons. Similar to conventional chemical recycling, HCl can separated from other effluents using a lime absorber.[9]
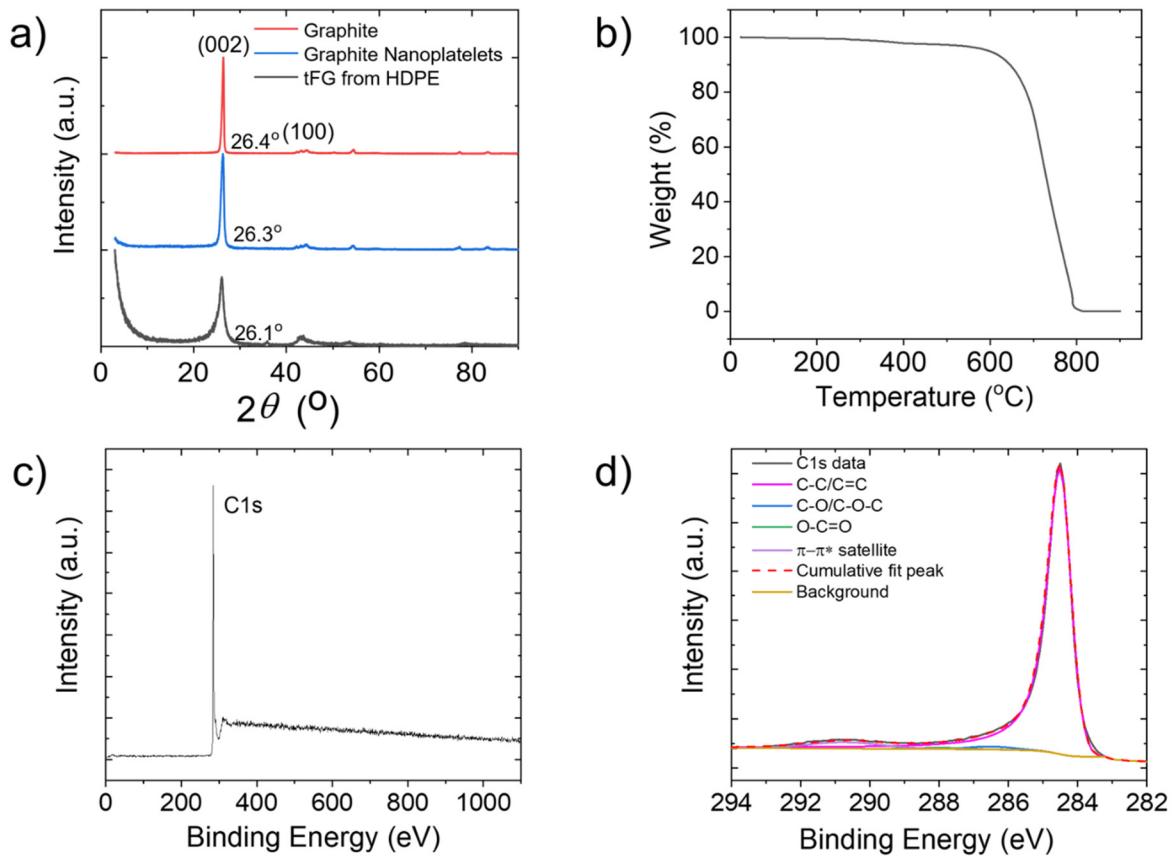
**Figure 3**. a) XRD of ACDC-tFG from HDPE. b) TGA (air, 15 °C/min) of ACDC-tFG from HDPE and c) Survey XPS scan of ACDC-tFG from HDPE. d) High resolution C1s XPS spectrum of ACDC-tFG from HDPE.

A TEM image of AC-FG shows highly graphitic sheets (Figure 4a) with an average size of 16 nm (Figure 4b). AC-FG are comprised of an average of 4 stacked turbostraic layers (Figure S23). From the TEM images, the spacing between the AC-FG layers was found to be 3.45 Å (Figure S24). Figure 4c shows a TEM image of ACDC-tFG with an average sheet size of 27 nm (Figure 4d), which is larger than that of the AC-FG. This suggests that following the AC-FJH process with DC-FJH promotes the lateral growth of the ACDC-tFG sheets. The increase in sheet size upon DC-FJH agrees with the decrease in the D band in the Raman spectra, because the intensity of the D band correlates to the surface to edges density; smaller graphene sheets often have higher D band intensities. DC-FJH was observed to result in an increase in the number of stacked FG sheets. TEM images of ACDC-tFG shows an average of 6 layers (Figure S25) of tFG per sheet with an average interlayer spacing of 3.45 Å. The interlayer distance calculations from the TEM images are included in Figure S26. The interlayer distance from the TEM images agrees with the XRD and Raman data that support the conclusion of the turbostratic morphology of ACDC-tFG.
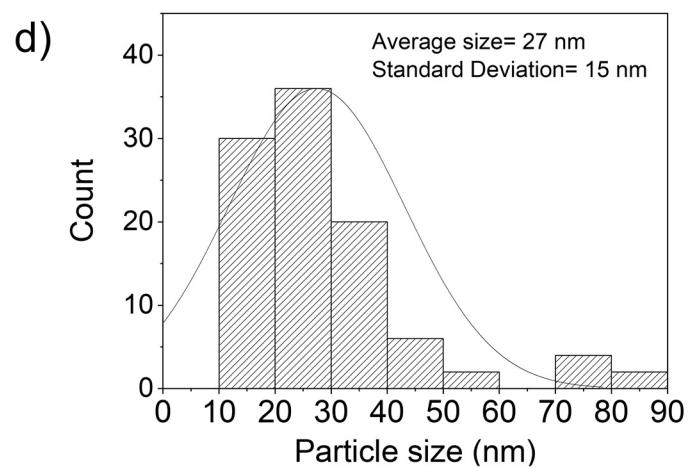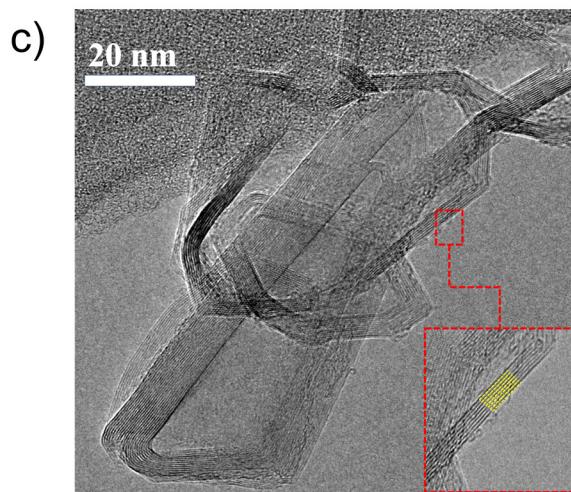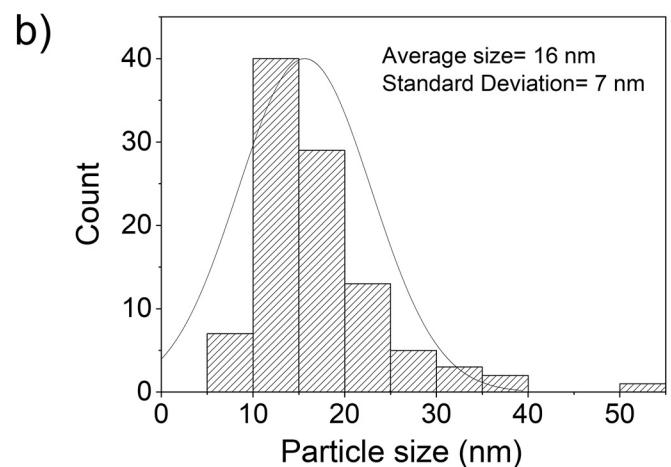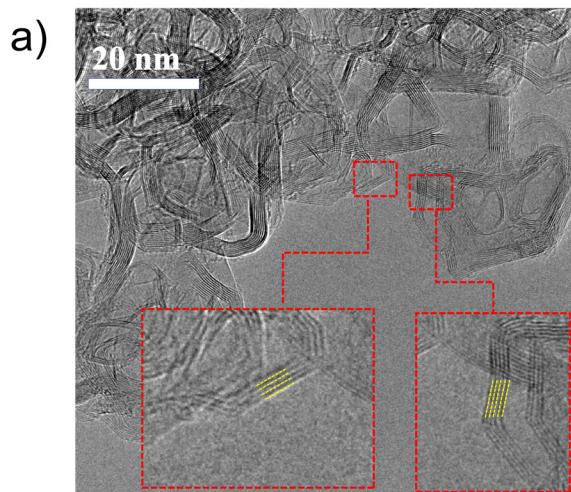
**Figure 4**. a) TEM image of AC-FG from HDPE and b) particle count of AC-FG (n = 100). c) TEM image of ACDC-tFG from HDPE and c) particle count of ACDC-tFG from HDPE (n = 100).

To calculate the energy required to covert mixed PW to FG, the resistivity across the sample was monitored during the FJH. The resistivity across the sample was observed to drop with time as shown in Figure 5a.

Starting from 1.0 g of mixed PW, with 40% HDPE, 20% PP, 20% PET, 10% LDPE, 8% PS, and 2% PVC, which is 81 wt% carbon content (the remainder being H, O and Cl), the mixed PW forms 0.18 g (22% yield) of intermediate AC-FG with the remainder being volatilized compounds; some waxes were isolated from the sidewalls of the quartz tube (see below). The conversion of the 0.18 g of intermediate AC-FG into high quality ACDC-tFJH graphene is nearly quantitative, hence there is a 22% overall yield of high-quality tFG from mixed PW following the combination ACDC-FJH protocol. When we start with 1.0 g of HDPE instead of mixed PW, the yield is 0.23 g (27% yield since HDPE is wt 86% carbon) of high-quality tFG after ACDC-FJH. We presume that the yield of graphene can be substantially increased if we build a pressure vessel that can retain more of the volatile components during the FJH steps for higher overall conversion.

The energy consumed during the AC-FJH processes is ~21 kJ/g. The energy required for the DC-FJH is ~13 kJ/g, but we are only DC-FJH 0.18 g of the original 1.0 g of mixed plastic. In total, 23 kJ is required to convert 1.0 g of mixed PW into 0.18 g of high-quality tFG. The energy calculation is shown in Figure S27. This translates to $124 in electricity cost to convert 1 ton of PW into 180 kg of high-quality tFG plus volatiles. This makes the cost of upcycling plastic using this technology competitive when compared to conventional physical and chemical recycling technologies. Currently, recycling technologies are not economical, which results in producing recycled plastic that is higher in cost than virgin plastic. This in turn leads to favoring the consumption of virgin plastic over recycled plastic, increasing plastic pollution and greenhouse gas emissions (see Table S1 for prices of recycled and virgin plastics).

Figure 5a gives insight into the mechanism of formation of tFG. Prior to voltage application in the AC-FJH, we start with a HDPE and CB mixture with high resistivity (low conductivity). As we proceed with AC-FJH, the current flows *via* the conductive CB generating a large amount of heat that carbonizes the non-conductive plastic causing the resistivity to drop with time, forming carbon rich AC-FG by the end of the AC-FJH process. At this point, evident by the collected Raman spectra in Figure 2a, AC-FG is not fully graphitized and exhibits a considerable amount of disorder, indicating that most of the applied energy in the AC-FJH process is applied towards carbonizing plastics by removing volatiles rather than graphitizing it. Upon DC-FJH of AC-FG, the current is uniform across the AC-FG, generating heat that graphitizes and heals the defects and disorder present in the AC-FG to obtain high quality tFG by the end of the ACDC-FJH process.[19,35]

The degree of graphene dispersibility is one of the important parameters that influences the processability of graphene into composites. Pluronic surfactants are low in price and often used to make stable aqueous graphene dispersions because of their hydrophilic tails and hydrophobic cores.[42, 43] The dispersibility of FG was studied in 1% aqueous Pluronic F-127 solution to find that dispersions with concentrations up to 1.2 mg/mL were attainable with AC-FG as shown in Figure 5b. ACDC-tFG dispersions were lower in concentration than that of AC-FG, which could be due to the larger sheet size of ACDC-tFG compared to AC-FG. However, both AC-FG and ACDC-tFG dispersion concentrations are significantly higher than many concentrations reported in the literature.[42-44] The ability to achieve FG dispersions with high concentration is likely due to the turbostratic morphology that makes is easier to overcome weaker Van der Waals interactions between the FG layers. When working with graphite, exfoliation of the layers only occurs when the net surface energy of the graphene and the solvent is greater than the strong Van der Waal

interactions between the AB-stacked layers.[45] For this reason, graphene dispersion from graphite usually requires costly organic solvents and high sonication power, which are not required for tFG dispersions. Therefore, dispersions made from graphite had much lower concentrations than those from tFG, making the utilization of tFG dispersions highly advantageous (Figure 5b). Secondly, the results here have not been industrially optimized, and would likely gain by using a pressure cell have the escaping gases also convert to graphene.

In addition, nano-sized tFG particles make it easy to disperse tFG in the presence of a small amount of surfactant. The quality of tFG was benchmarked against the quality of commercial graphene available on the market. tFG was found to have a significantly better Raman spectrum with a sharper 2D band and lower D band intensity (Figure 5c). Also, tFG has much better dispersibility than commercial graphene indicating that tFG has better processability into composites than commercial graphene. Given that the 98% of all graphene supplies are currently offering low quality graphene,[46] producing tFG from PW on a commercial scale could potentially elevate the quality of graphene available on the market and accelerate the transition of graphene-related technologies from laboratories to large scale industries. To demonstrate the usefulness of tFG, Portland cement composites of tFG derived from HDPE were tested to find that adding 0.035 wt% of FG from HDPE increases the compressive strength of Portland cement by 30% (Figure 5d). This is due to the increased integrity of calcium-silicate-hydrates in cement *via* addition of tFG.[47] Such enhancement in the compressive strength by adding small fractions of tFG is difficult to achieve with graphite or carbon fiber. For example, adding 0.05 wt% graphite to cement, which is almost double the loading of tFG in our composites, did not result in a noticeable change in the compressive strength.[48] This shows the advantage of the tFG in large scale applications where

17

small graphene loading translates into significant enhancement in the physical properties of composites.
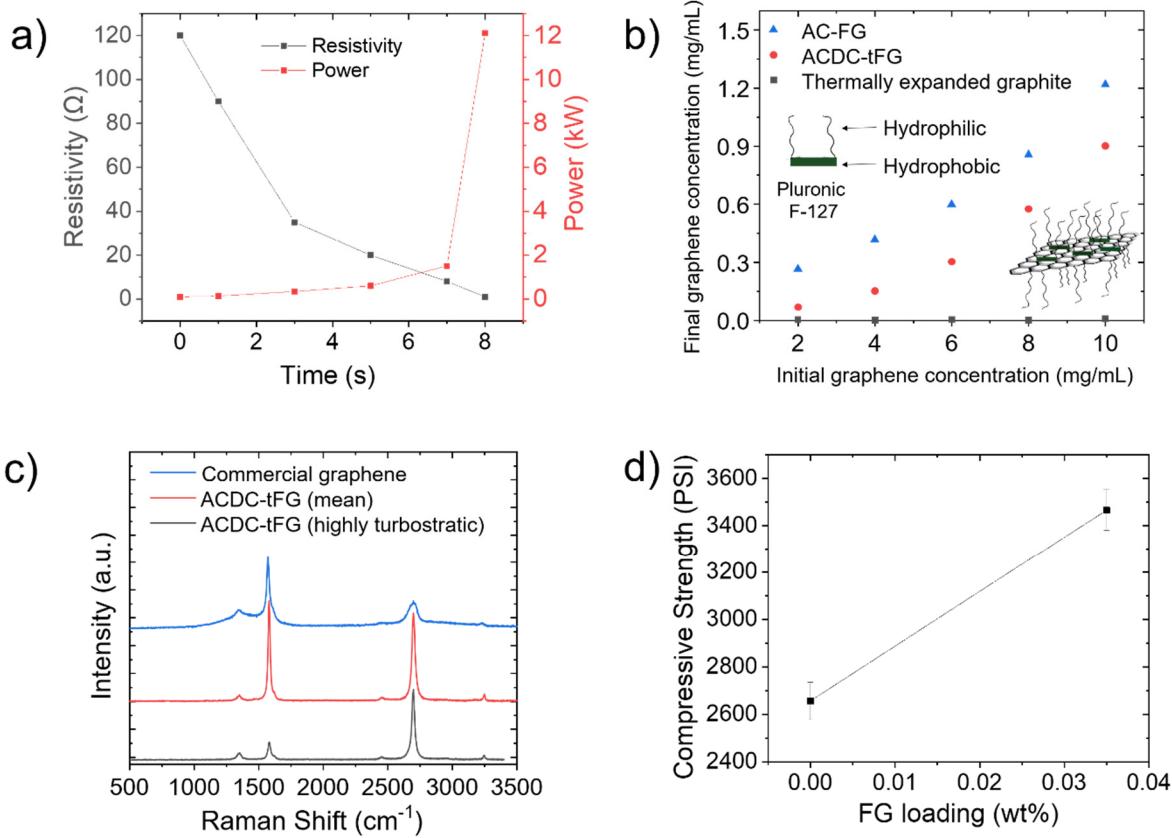


**Figure 5**. a) Resistivity values and power consumed during the AC-FJH process of HDPE. b) Bath-sonicated dispersions concentration of thermally expanded graphite, AC-FG and ACDC-tFG from HDPE and in 1% Pluronic before (initial) and after (final) centrifugation. c) Raman spectra of ACDC-tFG (from HDPE) and commercial graphene. d) Compressive strength cement/AC-FG composites (FG from HDPE).

The waxy substances formed during the AC-FJH process were collected and analyzed by FTIR to find that the waxes are oligomers with FTIR fingerprints similar to the parent plastic with a low degree of oxidation as shown in Figure 6. A schematic of the wax trap setup is shown in Figure

S28. These oligomers can be mixed with petroleum hydrocarbon streams for processing into virgin plastic or can be used to produce additives for detergents composites. The yield of oligomers is <10% indicating that ~60% of the flashed PW is transformed into gaseous product. To analyze the composition of the generated gases, a flashing electrode with a central hole drilled on the electrode face and a 90° turn to permit volatiles to escape was built (Figure S29). The gases evolved during FJH of HDPE were captured and collected in a cold trap. An estimate of the effluent composition was calculated based on the vapor pressures of the volatile stream at -196 °C; -78 °C (dry ice bath); 23 °C and 60 °C, indicating that the process affords $H_2:C_{1-3}:C_{4-6}$ in a 5:4:1 pressure ratio (not molar ratio). If a similar amount of $H_2$ remains to be generated upon scaling, then the $H_2$ might be used in a fuel cell to generate clean supplemental electricity for the FJH process.
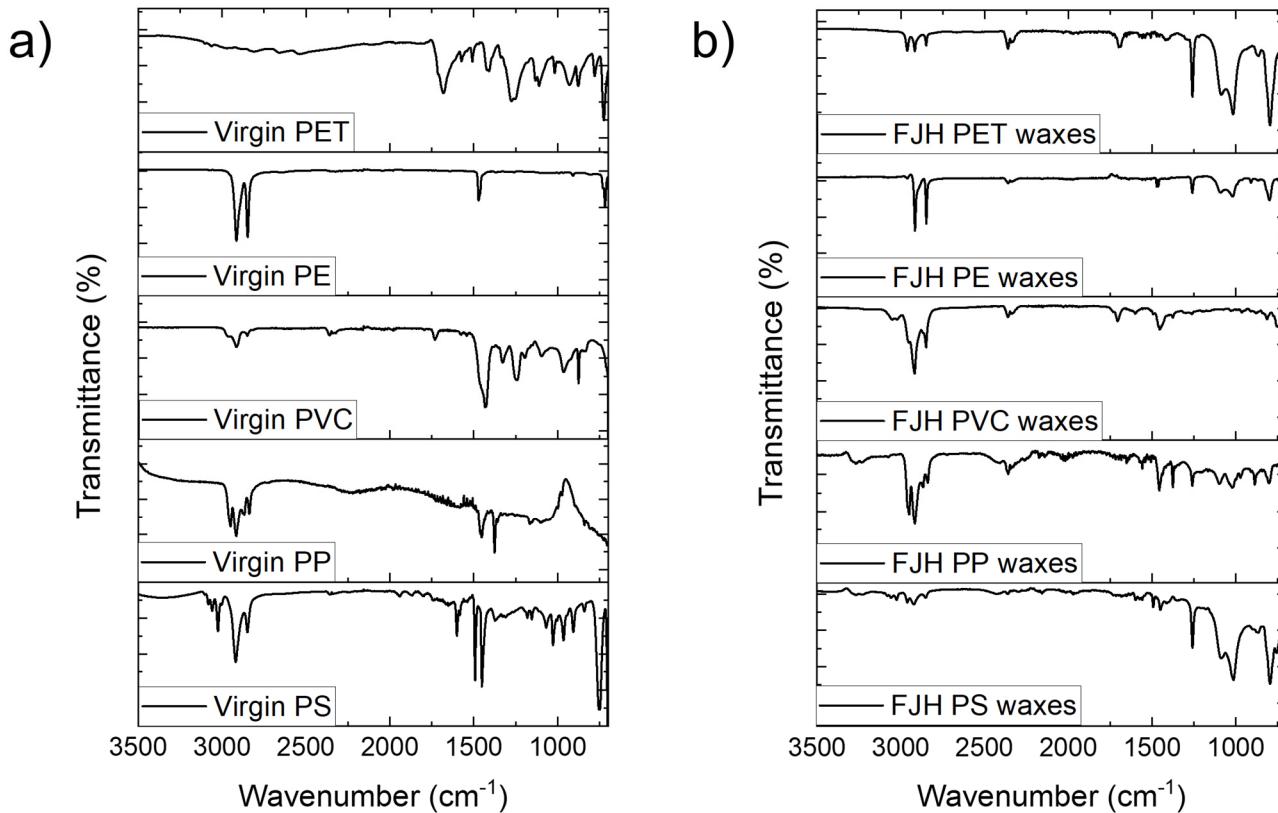


**Figure 6**. a) IR spectra of the plastics before and b) waxes after AC-FJH.

**Conclusions**

The ability to use small amounts of electricity to convert PW to higher value materials moves the world closer toward plastic neutrality. Using the FJH technology on a large scale to handle PW could potentially reduce the emissions of greenhouse gases in cradle to upcycle use of plastics,[7, 8, 18] however, a full life-cycle analysis remains to be done for the full utility of this approach. It has been reported that the production of 1 g of virgin PET requires 38.8 kJ of energy,[49] whereas treating PW using the FJH method will consume only 23 kJ, and this is for upcycling to tFG rather than merely recycling. Graphene is known to be a stable from of carbon with an extremely resilient structure. As with graphite, graphene can be slow in microbial degradation,[20, 21] thereby lessening re-entry into the carbon cycle. Therefore, FJH of PW should be considered as a method to upcycle PW.

**Methods**

**Materials.** CB (average diameter 10 nm, Black Pearls 2000) was purchased from Cabot Corporation. Recyclable PW was collected and separated based on type. The PW products reported in this work include PET from carbonated beverage bottles, HDPE from milk jugs or Polywize (Jacksonville TX), PVC from plumbing pipes, LDPE from single use plastics bags, PP from disposable straws and food packaging, and PS from disposable coffee cups. The PW was sanded or cut using a Shanghai Ke Heng Industrial Co. cutter to obtain powders with grain sizes 1 to 2 mm. The powdered plastic was then mixed with 5 wt% CB to obtain a conductive mixture. One could substitute CB with FG made in a prior reaction. In some cases used here, HDPE powder with grain size smaller the 50 µm was purchased as virgin material from Millipore-Sigma.

**AC-FJH**. Powders were packed between two copper electrodes in quartz tubes (tube thickness: 2 mm, inner diameter: 8 mm, length: 5 cm). The samples were compressed to obtain a resistivity of 120 to 125 $\Omega$ for 0.5 g of plastic. Alternating current (120 V, 60 Hz) was applied to the sample ~8 s in a vacuum desiccator (~10 mm Hg) to aid with outgassing. A detailed description of the AC system can be found in Figure S2.

**DC-FJH.** DC-FJH was performed on samples after AC-FJH. A capacitor bank composed of 10 capacitors of 450 V, and 60 mF, was charged to 110 V and allowed 500 ms discharge time to obtain high quality FG. Description of the DC circuit can be found in Figure S1.

**Characterization**. Raman spectra were obtained by excitation with a 532 nm laser in a Renishaw Raman microscope with 50x objective lens. X-ray diffraction (XRD) was performed using a Rigaku D/Max Ultima II Powder XRD. Thermal gravimetric analysis (TGA) was performed on a Q50 TGA from TA Instruments. Transmission electron microscopy (TEM) images were acquired using JEOL 2100F field-emission gun TEM at 200 kV. X-ray photoelectron spectroscopy (XPS) spectra were collected with a PHI Quantera SXM Scanning X-ray Microprobe with a base pressure of $5 \times 10^{-9}$ Torr. Survey spectra were recorded using 0.5 eV step sizes with a pass energy of 140 eV. Elemental spectra were recorded using 0.1 eV step sizes with a pass energy of 26 eV. Fourier transform infrared (FTIR) spectra were collected using a Nicolet 6700 FTIR spectrometer from Thermo-Scientific equipped with a GoldenGate accessory.

**Dispersion preparations**. FG solutions were prepared at concentrations from 1 to 10 g.L$^{-1}$ by suspending FG in 1 wt% Pluronic F-127 solution and sonicating for 30 min to disperse FG. After sonication, the dispersions were centrifuged in Beckman Coulter Allegra X-12 centrifuge equipped with a 19 cm in radius rotor at 1500 rpm (470 RCF) for 30 min to remove aggregates. The supernatant was diluted 500 times and analyzed *via* UV-VIS (Shimazu UV-3600 plus). The

absorbance was recorded at 660 nm and an extinction coefficient of $\alpha_{660}$= 6600 $L \cdot g^{-1} \cdot m^{-1}$ was used to calculate the concentration of graphene in solution.

**Cement composites preparation.** FG with 1 wt% pluronic F-127 was shear mixed in water using a Silverson L5MA shear mixer for 15 min at the speed of 5000 rpm to create a dark dispersion. FG dispersions were mixed with Portland cement using a dispersion to cement ratio of 0.40. Next, the slurry was cast in 4.90 x 4.90 x 4.90 cm PTFE cube molds (for compressive strength) and were allowed to set for 24 h. The compressive strength was measured after 7 days using a Forney Variable Frequency Drive automatic machine with dual load cells.

**Acknowledgements**

**Supporting Information Available**

Schematic of AC-FJH equipment, Raman spectra, energy conversion calculations and other graphs and data. This material is available free of charge *via* the Internet at http://pubs.acs.org.

**Conflicts of Interest**

Rice University owns intellectual property on the FG process which has been licensed to Universal Matter Ltd. JMT is a stockholder in Universal Matter Ltd. but not an officer or director. Conflicts of interest are managed by regular disclosure to the Rice University Office of Sponsored Programs

and Research Compliance. C-Crete Technologies owns intellectual property on the strengthening of graphene–cement/concrete composites.

## References

1.      Barnes, S. J. Understanding Plastics Pollution: The Role of Economic Development and Technological Research. *Environ. Pollut*. **2019**, *249*, 812-821.

2.      Sharma, S.; Chatterjee, S. Microplastic Pollution, a Threat to Marine Ecosystem and Human Health: A Short Review. *Environ. Sci. Pollut. Res.* **2017**, *24*, 21530-21547.

3.      Tetu, S. G.; Sarker, I.; Schrameyer, V.; Pickford, R.; Elbourne, L. D. H.; Moore, L. R.; Paulsen, I. T. Plastic Leachates Impair Growth and Oxygen Production in Prochlorococcus, the Ocean's Most Abundant Photosynthetic Bacteria. *Commun. Biol.* **2019**, *2*, 184-193.

4.      Lithner, D.; Nordensvan, I.; Dave, G. Comparative Acute Toxicity of Leachates from Plastic Products Made of Polypropylene, Polyethylene, PVC, Acrylonitrile–Butadiene–Styrene, and Epoxy to Daphnia Magna. *Environ. Sci. Pollut. Res.* **2012**, *19*, 1763-1772.

5.      Prata, J. C. Airborne Microplastics: Consequences to Human Health? *Environ. Pollut.* **2018**, *234*, 115-126.

6.      Cox, K. D.; Covernton, G. A.; Davies, H. L.; Dower, J. F.; Juanes, F.; Dudas, S. E. Human Consumption of Microplastics. *Environ. Sci. Technol.* **2019**, *53*, 7068-7074.

7.      Zheng, J.; Suh, S. Strategies to Reduce the Global Carbon Footprint of Plastics. *Nat. Clim. Change.* **2019**, *9*, 374-378.

8.      Dormer, A.; Finn, D. P.; Ward, P.; Cullen, J. Carbon Footprint Analysis in Plastics Manufacturing. *J. Cleaner Prod*. **2013**, *51*, 133-141.

9.      Al-Salem, S. M.; Lettieri, P.; Baeyens, J. Recycling and Recovery Routes of Plastic Solid Waste (PSW): A Review. *Waste Manage.* **2009**, *29*, 2625-2643.

10.     Hopewell, J.; Dvorak, R.; Kosior, E. Plastics Recycling: Challenges and Opportunities. *Proc. R. Soc. Lond.* **2009**, *364*, 2115-2126.

11.     Awasthi, A. K.; Shivashankar, M.; Majumder, S. Plastic Solid Waste Utilization Technologies: A Review. *IOP Conf. Ser. Mater. Sci. Eng.* **2017**, *263*, 022024.

12.     Panda, A. K. Thermo-Catalytic Degradation of Different Plastics to Drop in Liquid Fuel Using Calcium Bentonite Catalyst. *Int. J. Ind. Chem.* **2018**, *9*, 167-176.

13.     Kumar, S.; Singh, R. K. Recovery of Hydrocarbon Liquid from Waste High Density Polyethylene by Thermal Pyrolysis. *Braz. J. Chem. Eng.* **2011**, *28*, 659-667.

14.     Kiran Ciliz, N.; Ekinci, E.; Snape, C. E. Pyrolysis of Virgin and Waste Polypropylene and its Mixtures with Waste Polyethylene and Polystyrene. *Waste Manage.* **2004**, *24*, 173-181.

15.     Budsaereechai, S.; Hunt, A. J.; Ngernyen, Y. Catalytic Pyrolysis of Plastic Waste for the Production of Liquid Fuels for Engines. *RSC Adv.* **2019**, *9*, 5844-5857.

16.     Eriksson, O.; Finnveden, G. Plastic Waste as a Fuel - $CO_2$-Neutral or Not? *Energy Environ. Sci.* **2009**, *2*, 907-914.

17.     Gibb, B. C. Plastics are Forever. *Nat. Chem.* **2019**, *11*, 394-395.

18.     Geyer, R.; Jambeck, J. R.; Law, K. L. Production, Use, and Fate of All Plastics Ever Made. *Sci. Adv.* **2017**, *3*, e1700782.

19.     Luong, D. X.; Bets, K. V.; Algozeeb, W. A.; Stanford, M. G.; Kittrell, C.; Chen, W.; Salvatierra, R. V.; Ren, M.; McHugh, E. A.; Advincula, P. A.; Wang, Z.; Bhatt, M.; Guo, H.; Mancevski, V.; Shahsavari, R.; Yakobson, B. I.; Tour, J. M. Gram-Scale Bottom-Up Flash Graphene Synthesis. *Nature* **2020**, *577*, 647-651.

20.     Krishnamurthy, A.; Gadhamshetty, V.; Mukherjee, R.; Chen, Z.; Ren, W.; Cheng, H. M.; Koratkar, N. Passivation of Microbial Corrosion Using a Graphene Coating. *Carbon* **2013**, *56*, 45-49.

21.     Hsieh, Y. P.; Hofmann, M.; Chang, K. W.; Jhu, J. G.; Li, Y. Y.; Chen, K. Y.; Yang, C. C.; Chang, W. S.; Chen, L. C. Complete Corrosion Inhibition through Graphene Defect Passivation. *ACS Nano* **2014**, *8*, 443-448.

22.     Novoselov, K. S.; Fal'ko, V. I.; Colombo, L.; Gellert, P. R.; Schwab, M. G.; Kim, K. A Roadmap for Graphene. *Nature* **2012**, *490*, 192-200.

23.     Nan, H. Y.; Ni, Z. H.; Wang, J.; Zafar, Z.; Shi, Z. X.; Wang, Y. Y. The Thermal Stability of Graphene in Air Investigated by Raman Spectroscopy. *J. Raman Spectrosc.* **2013**, *44*, 1018-1021.

24.     Li, Y.; Feng, L.; Shi, X.; Wang, X.; Yang, Y.; Yang, K.; Liu, T.; Yang, G.; Liu, Z. Surface Coating-Dependent Cytotoxicity and Degradation of Graphene Derivatives: Towards the Design of Non-Toxic, Degradable Nano-Graphene. *Small.* **2014**, *10*, 1544-1554.

25.     Marta, d. A.; Andrea, L.; Marco, F.; Silvia, G. Toxicity Assessment of Laser-Induced Graphene by Zebrafish During Development. *J. Phys. Mater.* **2020**, *3*, 034008.

26.     Ferrari, A. C. Raman Spectroscopy of Graphene and Graphite: Disorder, Electron–Phonon Coupling, Doping and Nonadiabatic Effects. *Solid State Commun.* **2007**, *143*, 47-57.

27.     Cançado, L. G.; Takai, K.; Enoki, T.; Endo, M.; Kim, Y. A.; Mizusaki, H.; Jorio, A.; Coelho, L. N.; Magalhães-Paniago, R.; Pimenta, M. A. General Equation for the Determination of the Crystallite Size $L_a$ of Nanographite by Raman Spectroscopy. *Appl. Phys. Lett.* **2006**, *88*, 163106.

28.     Pimenta, M. A.; Dresselhaus, G.; Dresselhaus, M. S.; Cançado, L. G.; Jorio, A.; Saito, R. Studying Disorder in Graphite-Based Systems by Raman Spectroscopy. *Phys. Chem. Chem. Phys.* **2007**, *9*, 1276-1290.

29.     Schmucker, S. W.; Cress, C. D.; Culbertson, J. C.; Beeman, J. W.; Dubon, O. D.; Robinson, J. T. Raman Signature of Defected Twisted Bilayer Graphene. *Carbon* **2015**, *93*, 250-257.

30.     You, Y.; Ni, Z.; Yu, T.; Shen, Z. Edge Chirality Determination of Graphene by Raman Spectroscopy. *Appl. Phys. Lett.* **2008**, *93*, 163112.

31.     Kim, K.; Coh, S.; Tan, L. Z.; Regan, W.; Yuk, J. M.; Chatterjee, E.; Crommie, M. F.; Cohen, M. L.; Louie, S. G.; Zettl, A. Raman Spectroscopy Study of Rotated Double-Layer Graphene: Misorientation-Angle Dependence of Electronic Structure. *Phys. Rev. Lett.* **2012**, *108*, 246103.

32.     Garlow, J. A.; Barrett, L. K.; Wu, L.; Kisslinger, K.; Zhu, Y.; Pulecio, J. F. Large-Area Growth of Turbostratic Graphene on Ni(111) *via* Physical Vapor Deposition. *Sci. Rep.* **2016**, *6*, 19804-19815.

33.     Niilisk, A.; Kozlova, J.; Alles, H.; Aarik, J.; Sammelselg, V. Raman Characterization of Stacking in Multi-Layer Graphene Grown on Ni. *Carbon* **2016**, *98*, 658-665.

34.     Hwang, J. S.; Lin, Y. H.; Hwang, J. Y.; Chang, R.; Chattopadhyay, S.; Chen, C. J.; Chen, P.; Chiang, H. P.; Tsai, T. R.; Chen, L. C.; Chen, K. H. Imaging Layer Number and Stacking Order Through Formulating Raman Fingerprints Obtained From Hexagonal Single Crystals of Few Layer Graphene. *Nanotechnology* **2012**, *24*, 015702.

35.     Stanford, M. G.; Bets, K. V.; Luong, D. X.; Advincula, P. A.; Chen, W.; Li, J. T.; Wang, Z.; McHugh, E. A.; Algozeeb, W. A.; Yakobson, B. I.; Tour, J. M. Flash Graphene Morphologies. *ACS Nano* **2020**, *ASAP*. DOI: 10.1021/acsnano.0c05900.

36.    Vodakov, Y. A.; Mokhov, E. N.; Ramm, M. G.; Roenkov, A. D. Epitaxial Growth of Silicon Carbide Layers by Sublimation Sandwich Method (I) Growth Kinetics in Vacuum. *Krist. Tech.* **1979**, *14*, 729-740.

37.    Abrahamson, J. Graphite Sublimation Temperatures, Carbon Arcs and Crystallite Erosion. *Carbon* **1974**, *12*, 111-141.

38.    Majdzadeh-Ardakani, K.; Zekriardehani, S.; Coleman, M. R.; Jabarin, S. A. A Novel Approach to Improve the Barrier Properties of PET/Clay Nanocomposites. *Int. J. Polym. Sci.* **2017**, 7625906.

39.    Lin, J.; Peng, Z.; Liu, Y.; Ruiz-Zepeda, F.; Ye, R.; Samuel, E. L. G.; Yacaman, M. J.; Yakobson, B. I.; Tour, J. M. Laser-Induced Porous Graphene Films from Commercial Polymers. *Nat. Comm.* **2014**, *3*, 5714.

40.    Li, Z. Q.; Lu, C. J.; Xia, Z. P.; Zhou, Y.; Luo, Z. X-ray Diffraction Patterns of Graphite and Turbostratic Carbon. *Carbon* **2007**, *45*, 1686-1695.

41.    Warren, B. E. X-Ray Diffraction in Random Layer Lattices. Phys. Rev. 1941, 59, 693-698.

42.    Lotya, M.; King, P. J.; Khan, U.; De, S.; Coleman, J. N. High-Concentration, Surfactant-Stabilized Graphene Dispersions. *ACS Nano* **2010**, *4*, 3155-3162.

43.    Seo, J.-W. T.; Green, A. A.; Antaris, A. L.; Hersam, M. C. High-Concentration Aqueous Dispersions of Graphene Using Nonionic, Biocompatible Block Copolymers. *J. Phys. Chem. Lett.* **2011**, *2*, 1004-1008.

44.    Johnson, D. W.; Dobson, B. P.; Coleman, K. S. A Manufacturing Perspective on Graphene Dispersions. *Curr. Opin. Colloid Interface Sci.* **2015**, *20*, 367-382.

45.    Hernandez, Y.; Nicolosi, V.; Lotya, M.; Blighe, F. M.; Sun, Z.; De, S.; McGovern, I. T.; Holland, B.; Byrne, M.; Gun'Ko, Y. K.; Boland, J. J.; Niraj, P.; Duesburg, G.; Krishnamurthy,

S.; Goodhue, R.; Hutchison, J.; Scardaci, V.; Ferrari, A. C.; Coleman, J. N. High-Yield Production of Graphene by Liquid-Phase Exfoliation of Graphite. *Nat. Nanotechnol.* **2008,** *3*, 563-568.

46.     Kauling, A. P.; Seefeldt, A. T.; Pisoni, D. P.; Pradeep, R. C.; Bentini, R.; Oliveira, R. V. B.; Novoselov, K. S.; Castro Neto, A. H. The Worldwide Graphene Flake Production. *Adv. Mater.* **2018**, *30*, 1803784.

47.     Meng, W.; Khayat, K. H. Mechanical Properties of Ultra-High-Performance Concrete Enhanced with Graphite Nanoplatelets and Carbon Nanofibers. *Compos. B. Eng.* **2016**, *107*, 113-122.

48.     Shahsavari, R. Hierarchical Modeling of Structure and Mechanics of Cement Hydrate, PhD Thesis, MIT, Cambridge, 2011.

49.     Perugini, F.; Mastellone, M. L.; Arena, U. A Life Cycle Assessment of Mechanical and Feedstock Recycling Options for Management of Plastic Packaging Wastes. *Environ. Prog.* **2005**, *24*, 137-154.

**Table of contents graphic:**